ANATOMICAL STRUCTURE OVERRIDES TEMPERATURE CONTROLS ON MAGNESIUM UPTAKE - CALCIFICATION IN THE ARCTIC/SUBARCTIC CORALLINE ALGAE *LEPTOPHYTUM LAEVE* AND *KVALEYA EPILAEVE* (RHODOPHYTA; CORALLINALES)

Merinda C. Nash

Walter Adey

Department of Botany, National Museum of Natural History, Smithsonian Institution, Washington, DC, USA, 20560

Author for correspondence: nashm@si.edu

Running title: Magnesium and anatomy in coralline algae

Key words: Coralline algae, calcification, biomineralization, magnesium, temperature, proxy

Abstract

Calcified coralline red algae are ecologically key organisms in photic benthic environments. In recent decades they have become important climate proxies, especially in the Arctic and Subarctic. It has been widely accepted that Magnesium content in coralline tissues is directly a function of ambient temperature, and this is a primary basis for their value as a climate archive. In this paper we show for two genera of Arctic/Subarctic corallines, *Leptophytum laeve* and *Kvaleya epilaeve,* that previously unrecognized complex tissue and cell wall anatomy bears a variety of basal signatures for Mg content, with the accepted temperature relationship being secondary. The interfilament carbonate has lower Mg than adjacent cell walls and the hypothallial cell walls have the highest Mg content. The internal structure of the hypothallial cell walls can differ substantially from the perithallial radial cell wall structure. Using high-magnification Scanning Electron Microscopy and etching we expose the nm-scale structures within the cell walls and interfilament. Fibrils concentrate at the internal and external edges of the cell walls. Fibrils ~10 nm thick appear to thread through the radial Mg-calcite grains and form concentric bands within the cell wall. This banding may control Mg distribution within the cell. Similar fibril banding is present in the hypothallial cell walls but not the interfilament. Climate archiving with corallines can achieve greater precision with recognition of these parameters. This paper is part of a series of investigations on controls on Mg uptake and distribution within the crusts of a range of coralline genera.

Introduction

Understanding tissue complexity and the structural organization of cell wall calcification in coralline algae is important for many reasons, including the growing use of these organisms as climate proxies and concern for the ecological effects of ocean acidification. There is a burgeoning interest in using coralline crusts as environmental proxies for late Holocene temperature (Hetzinger et al. 2009, Gamboa et al. 2010, Halfar et al. 2010), arctic ice sheet coverage (Halfer et al. 2013) and pH changes with time (Krayesky-Self et al. 2016). Typically magnesium content is used as a key indicator of late Holocene temperature fluctuations (Adey et al. 2013). Yet despite this utilization of coralline carbonate crusts for proxy climate research, there has been little study of tissue and cellular-scale physiology as it relates to the distribution of magnesium within the crust. Nor are the basic mechanisms of calcification fully understood (Adey 1998). This is in stark contrast to the status of other calcifiers used for proxy work, e.g. corals (Barnes and Lough 1993), foraminifera (Bentov and Erez 2005) and bivalves (Wanamaker et al. 2008). However, these well-known climate proxies have little application in the Arctic Region of greatest climate change affects (Adey et al. 2013), and without a greater understanding of coralline calcification physiology, precision proxy analysis of temperature and other environmental conditions, using coralline algae, is limited.

One of the key roles of corallines is the building of carbonate substrate that underpins many ecosystems globally. For example, the thick bioherms found in coral reef structures (Adey 1978a, b, 1998), the extensive rhodolith beds off South American (Amado-Filho et al. 2012, Bahia et al. 2010) and Australian (Harvey et al. 2016) shores,

maerl substrate in the Mediterranean (Martin et al. 2014) and the dominant rocky benthos biostromes and rhodoliths in many Arctic and Subarctic environments (Adey et al. 2013). There are concerns that as atmospheric pCO_2 increases and consequent ocean acidification increases, there will be negative impacts on the capacity of corallines to continue building these important substrates (e.g. McCoy and Kamenos 2014). The pace of research on the effects of temperature and climate change on coralline algae has outpaced both the published data on anatomy and our understanding of the biochemical processes controlling their carbonate skeletal building. For developing reliable past climate proxy information using corallines and anticipating future climate change impacts on these keystone calcifiers, as with any other organism, it is first necessary to understand how these algae organize their tissues, build their skeleton and control cellular-scale magnesium content.

While numerous studies of coralline growth rates under a wide range of temperature and light conditions have been published (Adey and McKibben 1970, Adey 1970, 1973, Adey and Vassar 1975, Kamenos et al. 2008, Diaz-Pulido et al. 2014, Vásquez-Elizondo & Enríquez 2016), little attempt has been made to relate this information to calcification processes. Also, it is only recently, with the use of higher magnification scanning electron microscopy (SEM) (Adey et al. 2005, 2015a) that the earlier implications of anatomical complexity (Adey 1964, 1965,1966a, Cabioch and Giraud 1986) have been fully appreciated. It has been proposed that calcification is a result of locally elevated pH during photosynthesis leading to super-saturation and associated mineral precipitation (Ries 2010). However, some parasitic corallines lack photosynthetic pigments, and have

haustoria to derive nutrition from their hosts, yet present typical tissue and calcified wall structures (Adey and Sperapani 1971, Adey et al.1974). Also, anatomical and magnesium content studies of Arctic corallines demonstrate that growth continues in Arctic winter darkness (Halfar et al. 2011, Adey et al. 2013). There has been an experiment recording continued calcification at night and in the dark (experiment in progress) indicating that calcification is not likely a straight forward association with micro-saturation state, as seen in some algae (e.g., *Halimeda*, Adey 1998, Sinutok et al. 2012).

Following on from the classical coralline studies, maturing around the turn of the 19th century, Adey (1964, 1965,1966a,b) laid out the basic tissue-structured anatomy of crustose corallines, adding the epithallium, intercalary meristem and cellular elongation (while calcified) to the classical model of perithallium and hypothallium. Later, SEM (Adey et al. 2005, Adey et al.2012) demonstrated greater sub-tissue complexity and added the calcified cell wall components inner wall (IW) and interfilament (IF). In this paper, we rename the inner wall the cell wall and retain the terminology interfilament, noting this is equivalent to the middle lamella in higher plants (Esau 1953); interfilament has also been referred to as interstitial (Ragazzola et al. 2016). We use the abbreviations PCW and PIF (perithallial cell wall and perithallial interfilament) and HCW and HIF (hypothallial cell wall and interfilament) to designate the carbonate wall components. It should be noted that while the interfilament is a minor component of total calcification in the species of this paper, it can be a major component in some genera (Adey et al. 2013, 2015a).

In this paper, we show for the first time the cellular-scale and anatomical controls on magnesium distribution within the carbonate skeletons of two Arctic/Subarctic coralline species. These are *Leptophytum leave* (Stromfelt) Adey, and the epiphytic (and non-photosynthetic parasitic) *Kvaleya epilaeve* Adey and Sperapani, from the northern Labrador Coast. *L. leave* is photosynthetic and forms expansive, but thin crusts (to one mm in thickness) generally on shell fragments and pebbles in deeper water (Adey 1966a, 1970). *K. epilaeve* is an epiphytic parasite, lacking in photosynthetic pigment, and producing hypothallial haustoria that penetrate upper perithallial cells of *L. leave* (Adey and Sperapani 1971). It is similar in physiology to the North Pacific Subarctic parasite *Ezo epiyessoense* (Adey et al.1974), which, along with its host *Lithophyllum yessoense*, lies in a distantly related coralline group. *K. epilaeve* is the only known Arctic genus of algae (Adey et al. 2008) and is absent or of very limited occurrence in Subarctic waters, where the host continues to be abundant (Adey and Sperapani 1971). Understanding and contrasting calcification within these two species, both growing in the same temperature, light and pH conditions, offers an opportunity to examine the wide variance of Mg content as a function of skeletal anatomy and metabolic processes.

Methods

Sample collection and site information

The sample was collected on 22nd July 2013, at the commencement of Arctic summer, from 16-18 m depth at inner Port Manvers Bay, Labrador. The collection site lies at 56º 57.1' N; 61º 32.8' W., near the northern end of the 50 km long Port Manvers Run, a north/south passageway inside of S. Aulatsivik Island (Fig. 1A, C). Sea ice is extensive

from November through early July, and the inter-island passages and bays are covered with snow-covered land fast sea ice through much of that period. At the collection site, the bottom was a shell/pebble gravel bed primarily of shell fragments and pebbles encrusted with *L. leave*, *L. foecundum* and *Clathromorphum compactum*; scattered coarse rhodolith *Lithothamnion glaciale* and *Lithothamnion tophiforme* were also present (Fig. 1B, D). *K. epilaeve* occurred on *L. leave* and *L. leave* grew on both sides of the shell fragments. Salinity was measured using electronic induction instrumentation and was 30 ppt. November to July near surface water temperatures, below the sea ice, are within the -1.5 to -1.8º C range. Bottom summer temperature measured at the site on 22nd July 2013 was 0.5ºC. Since this is relatively early in the summer season, peak temperatures are likely to be between 3-5ºC (Adey et al. 2015) with a mean growing season temperature of ~ 2 º C. This mean estimate is based on measurements from eight sites in the region (182 km S to 35 km N) with surface to bottom temperature records for 1964 (Adey 1966c) and 2013 (Adey et al. 2015). These ranged from 1.9 to 5.6º C during summer at 15-20 m. The snow-covered land fast sea ice overlying the gravel rhodolith bed from which the samples were taken likely precludes significant solar energy from reaching the bottom for eight months of each year.

Rob Nash 8/9/17 12:54 PM
Deleted: B

Species identification was made by WHA. The original sample is 2013-11(1) at the National Museum of Natural History.

Analytical methods

Scanning electron microscopy- energy dispersive spectroscopy (SEM-EDS)

154 The CCA sample was fractured, mounted using carbon tape and platinum coated prior to
155 scanning electron microscopy energy dispersive spectroscopy (SEM-EDS). For these
156 analyses, we used a Zeiss UltraPlus field emission scanning electron microscope
157 (FESEM) equipped with an HKL electron backscatter diffraction (EBSD) operated at 15
158 kV, 11 mm working distance. SEM was carried out at the Australian National University
159 Centre for Advanced Microscopy. SEM-EDS was used for spot analyses to quantify the
160 elemental composition of representative parts of the CCA crust. A range of SEM settings
161 were used for imaging. The more common secondary (SE) electron showing topography,
162 backscatter electron imaging (BSE) which shows higher magnesium areas as darker
163 carbonate and is useful for rapid visual identification of mineral distribution.
164
165 A second round of EDS was undertaken using a NOVA NanoSEM FEI at the National
166 Museum of Natural History's Department of Mineralogy. Typically EDS measurements
167 are made using 15 kV (Nash et al. 2011) so that there is enough energy to dislodge
168 electrons from a range of elements, e.g. from lighter magnesium up to heavier strontium.
169 The EDS beam interacts with a roughly spherical-shaped region of carbonate beneath the
170 surface. This region is referred to as the interaction volume. At 15 kV the interaction
171 volume is ~ 3 μm in diameter whereas the average cell wall thickness ranges from only
172 500 nm up to ~2 μm (occasionally thicker, up to 3 μm). Interfilament in these species
173 may be only a few grains wide, 200-500 nm up to 2 μm. These narrow areas of interest
174 in contrast to the larger beam interaction volume, pose a problem for obtaining accurate
175 Mg measurements for only cell wall or interfilament. For example, a measurement of the
176 cell wall may include minor amounts of carbonate from the adjacent interfilament and

vice versa. Generally even with this beam crossover, in our experience 15 kV is sufficient to identify a significant offset in magnesium while still collecting information that may be of interest such as strontium levels. However, where there are only a few grains of interfilament, as in the *L. leave,* the 3 µm interaction volume is problematic. A range of EDS settings were tested aiming to reduce the beam interaction volume so that Mg content for each the cell wall and the interfilament could be individually measured without the beam crossing into the adjacent substrate. A setting of 7 kV, working distance 6.4 mm and 1 nA current was used to measure the interfilament grains in the *L. leave* with a count time of 20 seconds. The sample was carbon coated. This was calculated to have an interaction volume of <1 µm. These results are reported separately to the main data set.

Rob Nash 8/6/17 8:19 PM
Deleted: /

Sample preparation

Initially the crust was fractured using shears and mounted in superglue. After first imaging of the fractured crust, the sample was polished using 2000 gsm wet and dry sandpaper then sonic cleaned in unbuffered deionized water for 2 minutes. This preparation was used for SEM EDS measurements; 8-9 measurements were made for each carbonate type of interest. Subsequently the sample was sonic cleaned in unbuffered deionized water for 20 minutes. The deionized water has a pH of ~6.5. When cleaned for 2 minutes the surface is very lightly etched allowing differentiation between different Mg-calcite morphologies without altering the measured Mg content. After cleaning for 20 minutes there is a visible difference in the surface with much of the interfilament Mg-calcite and smaller grains removed allowing imaging of nm scale cellular structures.

X-ray diffraction methods

Powder XRD was carried out using a SIEMENS D501 Bragg-Brentano diffractometer equipped with a graphite monochromator and scintillation detector, using CuKα radiation. A subsample was broken off the edge of the crust. This piece included *L. leave* with surficial *K. epilaeve*. The sample was ground using a mortar and pestle. Fluorite was added as an internal standard. The sample was not bleached and acetone was not added during the grinding as this has been found to occasionally induce alteration and precipitation of other minerals in other coralline samples we have worked with. Scan interpretation for mol% $MgCO_3$ followed the methods described by Nash et al. (2013).

Temperature calibration

Data for the graph in figure 5 taken from Halfar et al. (2010, 2013).

Results

SEM imaging overview

The specimen of *L. laeve* encased an aragonite carbonate shell. (Fig. 2A). The crust is approximately 500 microns thick (Fig. 2B) with a basal hypothallus ~80 microns thick. *K. epilaeve* has been considered to be an adelphoparasite, a species very closely related to its host. Although diminutive, and superficially appearing as scattered white sand grains, *K. epilaeve* can densely coat *L. leave*. Although often appearing as densely crowded conceptacles, it can possess the full basic array of anatomical features: hypothallium, perithallium and epithallium (the latter mostly absent, Adey and Sperapani 1971) (Fig. 2B). *L. laeve* typically has an epithallium that is one cell layer of rounded ovoid, thin

225 walled cells that are often absent in SEM sections. The *K. epilaeve* grows directly on the
226 *L. laeve* meristem (Fig. 2C, D) and there was no evidence of excavation required (by
227 borers or grazers), prior to settlement. This suggests that unlike the typical sloughing
228 relationship with epiphytes wherein epithallium builds up under the epiphyte until it
229 sloughs off, the *L. leave* does not recognize *K. epilaeve* as foreign. The perithallial cell
230 walls of *L. laeve* contain radially-oriented grains of Mg-calcite; the interfilament is thin
231 and has carbonate grains randomly orientated in a plane parallel to the filament axis or
232 cell top/ bottom. The interfilament shows up strongly as stripes on vertical fracture
233 sections (Figs. 2B, C). Note for easiest viewing of the fine structures, the figure images
234 are best viewed on screen rather than in print.
235
236 The first layer formed by the *K. epilaeve* has angular grains parallel to the *L. laeve*
237 surface (Fig. 2E). The bottom part of the cell wall is without radial structure and has
238 submicron beads appearing to calcify along and within organic fibrils (Fig. 2E). Organic
239 fibrils are visible between the basal layer of *K. epilaeve* carbonate grains and the
240 meristem of the *L. leave* (Fig. 2F) suggesting a method of attachment in addition to the
241 haustoria developed by some hypothallial cells (Adey and Sperapani 1971). There were
242 no haustoria visible in our SEM sample. Fine radial grains typically observed in cells of *L.*
243 *leave* beneath the meristem were not apparent in the cell walls of the *L. laeve* meristem
244 (Fig. 2E,F) suggesting this surficial carbonate may have been altered or remineralised
245 during the attachment process.
246
247 *SEM-EDS*

Measurements for magnesium content in *Leptophytum leave* were undertaken on both the upper (side with conceptacles) and under (without conceptacles) crusts (Fig. 3A, D). The parasite, *Kvaleya epilaeve* was present on both surfaces (Fig. 2A, B Fig. 3A). Measurements of *K. epilaeve* were made on the underside.

The Mg content of the perithallial and hypothallial cell walls of *L. leave* was measured (Fig. 3 A-D) as well as what appeared to be a transitional cell type between the basal hypothallus and the typical perithallial cells (Fig. 2 D-F). These transitional cells are within the perithallus but have thin cell walls similar to the hypothallial cells. There are clear visual differences between the cell walls of the three cell types. The perithallial cell walls are 1-2 microns wide with clearly radial Mg-calcite (Fig. 2B, F). The basal hypothallial cells are elongated relative to the perithallial cells and their cell walls are narrower and do not always show radial cell wall structure (Fig. 2C). The transitional cells have elongate cells relative to the perithallus but less so than the hypothallus, and their cell walls are thinner, ~ 0.5 – 1 micron and do not show radial structures. The interfilament of *L. laeve* has only a single layer of Mg-calcite grains (Fig. 2B, F), as noted above showing as a thin line on longitudinal axial fractures; fractures along the interfilament appear as conspicuous vertical stripes (Figs. 2C).

The *K. epilaeve* in the portion of the sample mounted for SEM did not present the typical elongated hypothallial cells as shown by Adey and Sperapani (1971), as this cut is not longitudinally placed on a growing lobe. The key difference between the perithallus of the *L. laeve* and *K. epilaeve* was the presence of wide (1-2 microns) areas of interfilament

Rob Nash 8/9/17 12:59 PM
Deleted: 2

Rob Nash 8/9/17 12:59 PM
Deleted: 2

Rob Nash 8/9/17 12:59 PM
Deleted: , B

Rob Nash 8/9/17 1:00 PM
Deleted: 2

in the *K. epilaeve* (Fig. 3F, 4A, B). In many corallines (Adey et al. 2005), including the *L. laeve* studied for this paper there is only a single layer of interfilament grains, and these present as vertical stripes on vertical fractures (Fig. 3B). EDS measurements were taken for both the *K. epilaeve* cell wall and interfilament (Fig. 4A, B). As the interaction volume of the EDS beam is ~ 3 microns (Methods) and the cell wall and interfilament thickness range from 1-3 microns, the values measured for both may include small amounts of the other, although every effort was made to place the beam on the widest part of the appropriate band. A second set of measurements was taken for the *L. leave* cell wall and interfilament using lower kV and the results are reported separately.

Mg content

Bulk whole sample content of Mg, determined by powder XRD was 10.8 mol% $MgCO_3$ (Mg/Ca 0.13). The EDS-determined average Mg content ranged from 9.1 (*K. epilaeve* Perithallial interfilament) to 16.7 mol% $MgCO_3$ (*L. leave* upper Hypothallial cell wall), (Table 1, Fig.6). The highest measured individual Mg content, 19.6 mol% $MgCO_3$, was in the *L. leave* upper crust HCW. Generally the Mg content of interfilament was lower than cell walls, and perithallial cell walls had the highest Mg content. The lowest values were for the *K. epilaeve* PIF and PCW, 9.1 and 10.1 mol% $MgCO_3$ respectively, not significantly different at significance level of 0.05 but are significantly different at significance level of 0.1 (p= 0.068) (Table 2). Keeping in mind the values for the cell wall and interfilament include a small amount of carbonate from the other, we consider the p=0.068 result likely does represent a true significant difference between the two. The PCW for the *L. laeve* was slightly higher at 11.2 and 12.9 mol% $MgCO_3$ (under and

Rob Nash 8/9/17 1:01 PM
Deleted: A,

Rob Nash 8/9/17 1:04 PM
Deleted: 2

Rob Nash 8/9/17 1:04 PM
Deleted: 3

Rob Nash 8/6/17 8:26 PM
Moved down [1]: This XRD Mg content is within the range for average winter and summer Mg contents for *Clathromorphum compactum* collected from Arctic Bay, Kingitok and Quirpon (Halfar et al. 2011, 2013).

upper crust respectively), these were not significantly different from each other (p=0.112). The combined average of the upper and under *L. leave* cell walls (12.2 mol% $MgCO_3$) was significantly higher (p=0.025) than the *K. epilaeve* cell wall. However, comparing only the *L. leave* cell wall of the under crust, the same side as the *K. epilaeve,* there was no significant difference (p=0.124). The greatest difference between the upper and under *L. laeve* crust was found between the hypothallial cell walls. The under HCW averaged 12.3 mol% $MgCO_3$, whereas the upper HCW was 4.4 mol% higher at 16.7 mol% $MgCO_3$. The upper HCW was significantly higher than the *L. leave* PCW's but not different from the transitional CW's (15.6 mol% $MgCO_3$). Based on the graph in figure 5 this upper range of Mg would equate to temperatures above 9.3°C, more than double the known summertime highs at the sampling site.

The results for comparison of the cell wall and interfilament grains in the *L. leave* using 7 kV showed the interfilament, 8.5 mol% $MgCO_3$ (n=6), was significantly lower (p=0.001) than the cell wall, 11.1 mol% $MgCO_3$ (n=8).

Structural features

Cell wall

Within the radial Mg-calcite structure (PCW) of the *K. epilaeve*, a concentric banding pattern is present (Fig. 7 A-C). The radial Mg-calcite grains are not always one continuous long grain. The banding is aligned to the presence of organic fibrils that appear regularly throughout the PCW (Fig. 7B). Organic fibrils, ~10 nm thick, are parallel to the cell wall edges. These are spaced 30-40 nm apart throughout the middle of

330 the cell wall. It appears that the fibrils are mineralized. At the outer edges of the cell wall
331 the number of fibrils increases and appear as a dense mesh approaching a membrane (Fig.
332 7B, C) that is infilled with carbonate. The parallel fibrils are connected to the radial Mg-
333 calcite grains, appearing as if to continue through the grain (Fig. 7C), similar to fence
334 wire threading through fence posts at pre-defined spacing. There are also fibrils that
335 drape over the grains. Where the fibrils concentrate to a mesh, this is also calcified but
336 with smaller grains without regular shape. In the *K. epilaeve* interfilament (PIF), the
337 grains are aligned to the cell wall surface (Fig. 7C). Fibrils also run through the PIF and
338 attach to the interfilament grains but not with the regular pattern seen in the cell wall.
339 Looking at a cross section of the cell wall from the top down (Fig. 7D), the fibrils can be
340 seen to form a dense mesh.
341

342 Similar features are visible in the *L. laeve* PCW (Fig. 8A, B), although the organic fibrils
343 are not as well exposed. Possibly these cell wall grains are less susceptible to dissolution
344 in the etching treatment making it more difficult to expose the organic features. The
345 radial cell wall grains appear anchored to the external edge of the cell wall, immediately
346 adjacent the interfilament.
347
348 After etching for 20 minutes, more of the organic fibrils are exposed in the *K. epilaeve*
349 interfilament (Fig. 9A) revealing a porous membrane. PIF grains have angular edges in
350 contrast to the rounded sides of the cell wall grains. The *L. laeve* perithallial
351 interfilament has rice-grain shaped Mg-calcite flattened against the external side of the
352 cell wall (Fig. 9B) with attachment fibrils. Fibrils are visible stretching between the
353 flattened interfilament grains on adjacent cells (Fig. 9C).
354
355 Hypothallial cell walls at 200-500 nm wide are much thinner than perithallial cell walls
356 (Fig. 10 A-C). The HCW internal structure appears roughly radial (Fig. 10 A- C). But, the
357 radial structure is not always well developed with parts of the HCW exhibiting a distinct
358 break down the middle of the radial structures (Fig. 10C). There are fibrils parallel to the
359 cell wall appearing to go through the wall grains similarly to the perithallial cell walls.
360 Interfilament grains are present, as in perithallial cells (Fig. 10B, C). The HCW wall can
361 have two clearly defined morphologies (Fig. 10C). The wall adjacent to the interfilament
362 is narrowest at ~200 nm, has closely spaced organic fibrils and is poorly calcified
363 compared to the inner part of the wall (300-400 nm wide) and appears more like a
364 mineralized membrane. The wider inner part of the cell wall has radial grains but without

Rob Nash 8/9/17 12:52 PM
Deleted:

366 the well-defined shape of the PCW radial grains. Similar to the perithallial cell walls,
367 there are fibrils appearing to thread through the hypothallial cell wall grains.
368
369 The transitional cells between the hypothallus and perithallus have features from both
370 types present (Fig. 10D). The cell walls can be narrow, <200 nm, poorly mineralized
371 similarly to the outer part of the hypothallial cell wall. Parts of the cell wall resemble the
372 perithallial cell walls, with radial grains and wall width of nearly 1 micron, although
373 along the same wall this changes to ~200 nm wide and a poorly mineralized membrane.
374 The parallel fibrils are also present within the transitional cell walls. Interfilament grains
375 are present comparably to those between hypothallial and perithallial cells.
376
377 **Discussion**
378 *Site temperature, ecology and growth*
379 The site of collection for this specimen (Fig. 1A) is a pavement of coralline encrusted,
380 roughly flat to ovoid shells and pebbles often with dish shapes. Many, such as the
381 specimen employed in this study have a concave surface (due to the original mollusk
382 shape). The benthic surface that we show in figure 1B is likely quite stable with time in
383 the moderate reversing tidal current environment of the site. The conceptacles of *L. leave*,
384 requiring considerable solar energy for construction; all appear on the upper side of the
385 specimen and further assist our determination of orientation. Since the sea ice does not
386 clear the area until late June or early July, solar energy has already peaked, by the time
387 the benthos at 15-17 m receives significant light. Effectively, the growing season is July
388 through November, and with a mean growing season temperature of < 2º C. Based on the

Rob Nash 8/9/17 1:05 PM
Deleted: B

lateral growth rates (5-7 µm/day) found by Adey (1970), a season of lateral growth would provide less than one mm of extension. As we discuss below, the vertical growth in this species is slower than the lateral growth. The layering seen in figure 2B likely represents 4-5 years of vertical growth. At 80-100 µm of perithallial addition/year, this relates well to the 100-200 µm /year found with extensive data in the same region for *Clathromorphum compactum* (Adey et al. 2015b).

Rob Nash 8/9/17 1:06 PM
Deleted: 1

Considering that *Leptophytum leave* crusts can be many cm broad and rarely exceed 500 µm in thickness, except by overgrowing of earlier crusts, it can be assumed that after initial formation, upwards perithallial growth is either very slow, perhaps limited by the development of conceptacles for which considerable photosynthate must be dedicated. *L. leave* is a deep water species (Adey 1966a, b, 1968, 1971) and requires little solar energy to grow and carry out its life cycle; however, as shown by Adey (1970), the rate of hypothallial extension falls with light reduction, and it would be expected that growth on the underside of a shell-encased fragment would be present but less than that on the upper surface.

Temperature and magnesium

One of the challenges using samples collected at a single point in time is that the growth history cannot always be precisely tied to previous points in time and temperature. As discussed in the previous section, this crust likely represents 4-5 years of growth. Thus the XRD mol% $MgCO_3$ is an average for that period. The individual EDS measurement

spots cannot be tied to a particular time of year or temperature. However, the annual temperature range is not large, estimated to be ~ 4 ºC across the growing season.

The XRD Mg content is within the range for average winter and summer Mg contents for *Clathromorphum compactum* collected from Arctic Bay, Kingitok and Quirpon (Halfar et al. 2011, 2013). The EDS-determined average Mg content for each carbonate type had a range of 7.6 mol% $MgCO_3$, from 9.1 (*K. epilaeve* interfilament) to 16.7 mol% $MgCO_3$ (*L. laeve* upper crust hypothallus). The *L. laeve* upper hypothallus has 84% more Mg than the *K. epilaeve* interfilament. Although the exact time and temperature of formation for each component is not known, the temperature range (~4 ºC) alone is highly unlikely to explain the Mg difference. Studies on Mg content in CCA for temperature proxies have used regressions with temperature records to determine a range of responses from 0.266 mol % (Williamson et al. 2014), ~1.0 (Halfar et al. 2000; Darrenougue et al. 2013) to 1.76 mol% $MgCO_3$ (Kamenos et al. 2008) per degree celsius of temperature increase. Only the Kamenos et al. (2008) calibration is close to explaining the range here. However, that calibration was for branches of the rhodolith *Lithothamnion glaciale*. Using temperature calibrations for crust CCA in experimental treatments, where temperature was the only condition changed (Diaz-Pulido et al. 2014; Nash et al. 2016), a calibration of 0.33 mol%/°C is obtained. This rate is in agreement with results from Williamson et al. (2014), Chave and Wheeler (1964) and Adey (1965). Using 0.33, a shift of 7.6 mol% equates to 23°C of change, nearly four times greater than the maximum annual range at this site. The magnesium offsets in different parts of the crust are clearly aligned to anatomical features and not controlled by temperature. This proposal is

Rob Nash 8/6/17 8:26 PM
Moved (insertion) [1]

Rob Nash 8/6/17 8:26 PM
Deleted: is

supported by recent results for species of CCA *Phymatolithon* that also demonstrated anomalously higher Mg in hypothallial cells across four species collected from differeing locations (Nash and Adey 2017). Within these offsets there may still be a response to temperature over the seasons, but it was beyond the capacity of this study to investigate seasonal changes. It is noteworthy that the upper crust hypothallus average of 16.7 mol% $MgCO_3$ is equivalent to new surface crust of tropical *Porolithon onkodes* grown at 30° C (Diaz Pulido et al. 2014).

Structural features

There are three main types of calcified structures within the vegetative tissues of *Leptophytum leave* and *Kvaleya epilaeve*: (1) the radial Mg-calcite within the cell walls of the perithallium, (2) the interfilament in both the perithallium and hypothallium and (3) the thin hypothallial cell walls. Each has distinctively different features and magnesium content. The more elongate (and thinner-walled) cells of the hypothallus have been reported for other species of Melobesioideae (Adey 1964, 1965, 1966a). However, this is the first study to show that the internal cell wall Mg-calcite structure and their magnesium content differs from perithallial cell wall. Probably these thinner elongated hypothallial cell walls are a result of relatively rapid growth during lateral extension. There are numerous examples documenting higher Mg in parts of crusts that have grown faster during the warmer seasons (e.g. *Clathromorphum compactum* and *C. nereostratum* by Adey et al. 2013). In this case there is no elevated temperature. The mechanistic process by which more Mg is incorporated into the HCW and how this relates to growth rate is not known. The *K. epilaeve* perithallial cells had lower Mg than the *L. leave*

perithallial cells. Cabioch and Giraud (1986) described the *perithallial* cells as being a later stage of development than *epithallial* cells. Epithallial cells do not have fully developed rounded cell walls of the perithallial cells (Adey 2015a, b). Although Mg-content of epithallial carbonate is lower than the perithallial values (Diaz-Pulido et al. 2014, Nash et al. 2015, 2016), the lower Mg measured here is not considered a result of different cell type as the *K. epilaeve* cell walls have the radial calcite similarly to the perithallial *L. Leave*, indicating that these are similarly well developed. Considering the time of collection in early summer, it is quite possible that the *K. epilaeve* growth closest to the *L. leave* surface was laid down closer to winter and in cooler temperatures, this being a likely explanation for the lower Mg content.

Calcification and photosynthesis

The parasitic epiphyte *K. epilaeve* is not known to photosynthesize. The similarity of cell wall and interfilament features to those of the photosynthesizing host, *L. leave*, suggests that the precipitation of the Mg-calcite is not directly driven by photosynthesis as has been suggested for coralline algae (Ries 2010) and demonstrated for calcifying green algae *Halimeda*, (e.g. Adey 1998, Sinutok et al. 2012). Rather, considering also the evidence for continued calcification during the Arctic winter (Halfar et al. 2011, Adey et al. 2013), it seems likely the first control is the provision of the organic substrate that subsequently either becomes calcified or induces calcification. This does not negate the possibility of increased calcification as photosynthetic rates increase (e.g. Borowitzka 1981).

Banding and magnesium uptake

The concentric banding of organic fibrils within the perithallial cell wall is interesting from a magnesium perspective. The dominant visual morphological pattern is the radial Mg-calcite crystals. In contrast, other work indicates the dominant pattern of Mg distribution within the cell may be unrelated to the radial features. Concentric zonations of higher Mg content have been shown, using back scatter electron imaging, in cell walls of tropical *Porolithon onkodes* (Nash et al. 2011). Ragazzola et al. (2016) using NanoSIMs, also showed clear concentric banding of Mg within summer cell walls of *Lithothamnion glaciale*. These published observations together with the results in this study suggest there could be a strong organic control on Mg distribution within the cell, with this being related to the concentric fibrils. Possibly the fibril organics enable higher Mg incorporation than the organics involved in the radial structures. Ragazzola et al. (2016) further documented a decreased prominence of Mg banding in winter cells of *L. glaciale* and for those grown in CO_2 enriched conditions. Results from our study offer an insight as to possible temperature or CO_2-driven ultrastructure changes that may result in decreased Mg content. If the banded fibrils observed in this study are normally similarly present in the *L. glaciale,* then an absence of the Mg bands for their winter and elevated CO_2 treatment suggests that these fibrils could either be absent, or the organic structure or composition has changed and no longer enables elevated Mg.

Relevance to Climate Archiving

This study has several implications for climate archiving using corallines. Most importantly, anatomical controls can override temperature influences on Mg composition.

We do not suggest current studies are inadequate because the finer scale (submicron) scale variations are not captured. These fine scale variations will not change the general trends or conclusions. Rather, we suggest caution regarding interpretation of data where a change in Mg is visibly associated with a change in cell type as temperature may not be the only possible driver of Mg change. While hypothallial areas can usually be easily excluded from most climate archiving (but see Bougeois et al. 2015), less obvious anatomically different tissues such as the elevated Mg transitional cell walls may not be noticeable at low magnification. This may lead to a false positive result identifying such a region as reflecting a time of higher temperature. As well as these tissue-scale differences, the cellular scale differences may also need to be considered. Any seasonal change in relative proportion of CW to IF can shift the [Mg] in absence of any temperature-influenced change. For example if CW = 10 mol% $MgCO_3$ and IF = 8 mol% $MgCO_3$, and crust changes from 90:10 CW:IF to 50:50 this would equate to a change in of 9.8 to 9 mol% for measurements of bulk crust (i.e. spot sizes larger than the cell size, or smaller spot sizes averaged without reference to their anatomical placement). This change equates to a 2-3 degrees using a temperature calibration of 0.33 mol% $MgCO_3$ °C. Should the difference in cell wall and interfilament mol% $MgCO_3$ be larger, then the total average will change more substantially. Furthermore, the bulk magnesium results for different CCA species with differing proportions of cell wall:interfilament from the same temperature environments will have a range of non-temperature related Mg content that is controlled by the cell wall:interfilament. This change in structure, if seasonally correlated, will be indirectly related to temperature, but there may be other influences such as light.

Rob Nash 8/13/17 5:25 PM
Deleted: Thus, any study of CCA for temperature archiving must take into account changes in anatomy throughout the measured areas.

Thus, the best CCA temperature climate archives, as compared to seasonal archives, are likely to be those with the least seasonally varying ultrastructure changes.

Understanding the combined contribution of anatomical and temperature changes to measured magnesium may help explain the variation of Mg-temperature calibrations in the published literature. Typically it is the rhodoliths that show the highest response of Mg to temperature, e.g. *Lithothamnion glaciale* at 1- 1.76 mol% $MgCO_3$ (Halfar et al. 2000; Kamenos et al. 2008) per degree celsius of temperature increase compared to *Clathromorphum compactum* at 0.7 mol% $MgCO_3$ (Halfar et al. 2010). The *L. glaciale* has distinct seasonal changes shifting to a clear band of elongated cells during summer. The rhodolith summer cells have similarities in appearance to the hypothallial cells in this study. Possibly the higher measured Mg in the long cells of the rhodolith is a result in part of a switch towards a more perithallial style cell and may not be entirely temperature related. This proposition is supported by Sletten et al. (2017) who found a switch to elongated cells with higher Mg that was unrelated to seasonality. In contrast, anatomical changes in *C. compactum* (Adey et al. 2013) are not so extreme.

Suggestions for improving analytical methods

Our work is ongoing in this area of research and as more species and ultrastructure are studied we expect to be able to provide more detailed guidance on utilizing Mg from CCA for climate proxies. However, in the interim, there are several steps that could be incorporated into routine analyses to improve the accuracy of Mg climate proxies. Firstly, it should become a routine part of analyses that the ultrastructure is assessed to determine

555 if the ratio of cell wall to interfilament carbonate changes regularly with seasons. Second,
556 when possible as well as the larger spot sizes used in sampling transects, e.g. 10-20
557 microns, make discrete spot analyses using the smallest reliable interaction volume
558 possible to determine indicative Mg offsets between the cell wall and interfilament so
559 that this can be adjusted for if necessary, in the final interpretation. Third, ensure that
560 hypothallial growth is not included in sampling transects. Usually the basal hypothallus is
561 easily avoided, but secondary hypothallus and transitional cells may be harder to avoid
562 without careful SEM analysis.
563
564 **Conclusion**
565 It appears that within these CCA, there is a strong control on the uptake of Mg in relation
566 to the different anatomical components. This is in contrast to the suggestion by Ries
567 (2010), based on Mg:Ca in seawater manipulation experiments, that corallines exert little
568 or no control over their Mg uptake other than to specify the polymorph. Recent work
569 indicates that the interfilament and perithallial carbonate react similarly to temperature,
570 but the responsive hypothallial carbonate is inconclusive (Nash and Adey 2017). It would
571 be interesting to identify if each of interfilament, perithallial and hypothallial cell walls
572 reacted similarly to changes in seawater Mg:Ca, or if there were differences in anatomical
573 controls. Crucially, it is necessary to keep in mind the biological controls on Mg uptake
574 when using CCA Mg changes as a climate proxy.
575
576 While the focus of this study has been the distribution of Mg with different anatomical
577 features, the high-magnification images are the first to show the cellular-scale organic

Rob Nash 8/13/17 8:04 PM
Deleted: temperature and

structures together with the carbonate components. The orientation of the crystals in the interiflament and the cell walls are in agreement with lower-magnification SEM studies on a range of algal species (Cabioch and Giraud 1986, Adey et al. 2013). The combination of gentle etching and high-magnification SEM has revealed previously unknown features such as the fibrils threading through the radial Mg-calcite (Fig. 7C). Further, showing that the Mg content varies with anatomical features suggests that the calcification may be a different process, or have different controls, for each carbonate type. This adds an extra level of complexity when considering how environmental changes, such as increasing temperature, may impact on the capacity of the CCA to continue their important substrate provision ecological role.

Acknowledgments

Thanks to the Centre for Advanced Microscopy at the Australian National University and the Mineral Sciences department at the Smithsonian Institution for assistance with SEM-EDS.

References

Adey, W. 1964. The Genus *Phymatolithon* in the Gulf of Maine. *Hydrobiologia* 24:377-420.

Adey, W. 1965. The Genus *Clathromorphum* in the Gulf of Maine. *Hydrobiologia* 26:539-573.

Adey, W. 1966a. The Genera *Lithothamnium, Leptophytum* (nov. gen.) and P*hymatolithon* in the Gulf of Maine. *Hydrobiologia* 28:321-368.

602 Adey, W. 1966b. The Genus *Pseudolithophyllum* in the Gulf of Maine.
603 *Hydrobiologia* 27:479-597.
604 Adey, W. 1966c. The Distribution of Saxicolous Crustose Corallines in the
605 Northwestern North Atlantic. *J. Phycol.* 2:49-54.
606 Adey, W. 1970. The Effects of Light and Temperature on Growth Rates in
607 Boreal-Subarctic Crustose Corallines. *J. Phycol.* 6:269-276.
608 Adey, W. 1973. Temperature Control of Reproduction and Productivity in a
609 Subarctic Coralline Alga. *Phycologia* 12:111-118.
610 Adey, W. 1978a. Coral Reef Morphogenesis: A Multidimensional Model.
611 *Science* 202:831-837.
612 Adey, W. 1978b. Algal Ridges of the Caribbean Sea and West Indies. *Phycologia*
613 17:361-367.
614 Adey, W. 1998. Coral Reefs: algal structured and mediated ecosystems in shallow,
615 turbulent alkaline seas. *J. Phycol.* 34:393-406.
616 Adey, W. & D. McKibbin. 1970. Studies of the Maerl Species of the Ria de Vigo.
617 *Bot. Mar.* 8:100-106.
618 Adey, W. & C. Sperapani. 1971. The Biology of *Kvaleya epilaeve*, A New
619 Parasitic Genus and Species of Corallinaceae. *Phycologia* 10:29-42.
620 Adey, W., T. Masaki & H. Akioka. 1974. *Ezo epiyessoense*, A New Parasitic Genus and
621 species of Corallinaceae. *Phycologia* 13:329-344.
622 Adey, W. & J. M. Vassar. 1975. Colonization, Succession and Growth Rates of
623 Caribbean Crustose Corallines. *Phycologia* 14:55-69.

624 Adey, W., Y. Chamberlain, & L. Irvine. 2005. A SEM-Based Analysis of the
625 Morphology, reproduction and ecology of *Lithothamnion tophiforme* Unger
626 (Corallinales, Rhodophyta), an Arctic coralline. *J. Phycol*. 41:1010-1024.
627 Adey, W., Lindstrom, S., Hommersand M. & Muller, K. 2008. The biogeographic origin
628 of Arctic endemic seaweeds: A thermogeographic view. *J. Phycol.* 44:1384-1394.
629 Adey, W., Halfar, J. & Williams, B. 2013. The coralline genus *Clathromorphum* Foslie
630 emend Adey; biological, physiological and ecological factors controlling
631 carbonate production in an Arctic/Subarctic climate archive. *Smithsonian*
632 *Contributions to the Marine Sciences* 40:1-83.
633 Adey, W., Hernandez-Kantun, J. J., Johnson, G. & Gabrielson, P. 2015a. DNA
634 sequencing, anatomy and calcification patterns support a monophyletic, Subarctic,
635 carbonate reef-forming *Clathromorphu*m (Hapalidiaceae, Corallinales,
636 Rhodophyta). *J. Phycol.* 51:189-203.
637 Adey, W., Halfar, J., Humphreys, A. Belanger, D., Gagnon, P. & Fox, M. 2015b.
638 Subarctic rhodolith beds promote longevity of crustose coralline algal buildups
639 and their climate archiving potential. *Palaios* 30:281-293.
640 Amado-Filho, G., Moura, R., Bastos, A., Salgado, L., Sumida, P., Guth, A., Francini-
641 Filho, R., Pereira-Filho, G., Abrantes, D., Brasileiro, P., Bahia, R., Leal, R.,
642 Kaufman, L., Kleypas, J., Farina, M. & Thompson, F. 2012. Rhodolith Beds are
643 major CaCO3 bio-factories in the Tropical South West Atlantic. *Plos One* 7
644 (4):e35171.

Bahia, R., Abrantes, D., Brasileiro, P., Pereira-Filho, G. & Amado-Filho, G. 2010. Rhodolith bed structure along a depth gradient on the northern coast of Bahia State, Brazil. *Brazilian J. Oceanography* 58:323–337.

Barnes, D. J., & Lough, J. M. 1993. On the nature and causes of density banding in massive coral skeletons. *J. Exp. Mar. Biol. Ecol.* 167:91-108.

Bentov, S., & Erez, J. 2005. Novel observations on biomineralization processes in foraminifera and implications for Mg/Ca ratio in the shells. *Geology* 33:841-844.

Borowitzka, M. A. 1981. Photosynthesis and Calcificaton in the Articulated Coralline Red Algae *Amphiroa anceps* and *A. foliacea*. Mar. Biol. 62:17-23.

Bougeois, L., Williams, B., Halfar, J., Konar, B., Adey, W., Kronz, A. & Wortmann, U.G. 2015. Does the coralline alga *Leptophytum fœcundum* (Kjellman) capture paleoenvironmental variability in the Arctic Ocean? *Arctic, Antarctic, and Alpine Research* 47:375-387.

Chave, K. & B. Wheeler. 1965 Mineralogical changes during growth in the red alga *Clathromorphum compactum*. *Science* 147:621.

Darrenougue, N., De Deckker, P., Payri, C., Eggins, S., & Fallon, S. 2013. Growth and chronology of the rhodolith-forming, coralline red alga Sporolithon durum. *Marine Ecology Progress Series* 474:105-119.

Diaz-Pulido, G., Nash, M.C., Anthony, K.R., Bender, D., Opdyke, B.N., Reyes-Nivia, C. & Troitzsch, U., 2014. Greenhouse conditions induce mineralogical changes and dolomite accumulation in coralline algae on tropical reefs. *Nature communications*, *5*.

668 Esau, K. 1953. Plant Anatomy. John Wiley and Sons. New York. 735 pp.
669 Nash, M. C., Opdyke, B. N., Troitzsch, U., Russell, B. D., Adey, W. H., Kato, A., Diaz-
670 Pulido G., et al. 2013. Dolomite-rich coralline algae in reefs resist dissolution in
671 acidified conditions. *Nat. Clim. Change* 3:268-272.
672 Halfar, J., Zack, T., Kronz, A., & Zachos, J. C. 2000. Growth and high-resolution
673 paleoenvironmental signals of rhodoliths (coralline red algae)- A new biogenic
674 archive. *J. Geophysical Research* 105:22-107.
675 Gamboa, G., Halfar, J., Hetzinger, S., Adey, W., Zack, T., B. Kunz, B., & Jacob, D. 2010.
676 Mg/Ca ratios in coralline algae as proxies for NW Atlantic temperature variations.
677 *J. Geophysical Research-Oceans* 115:1-12.
678 Halfar, J., Hetzinger, S., Adey**,** W., Zack, T., Gamboa, G., Kunz, B., Williams, B., Jacob,
679 D. 2010. Coralline algal growth increment widths archive North Atlantic climate
680 variability. *Palaeogeography, Palaoeoclimatology, Palaeoecology* 302:71-80
681 Halfar, J., Adey, W., Kronz, A., Edinger, E., & W. Fitzhugh, W. 2013. Unprecedented
682 sea-ice decline archived by novel multi-century annual-resolution algal proxy.
683 *PNAS* 110: 197837-19741.
684 Harvey, A. S., Harvey, R. M., & Merton, E. 2016. The distribution, significance and
685 vulnerability of Australian rhodolith beds: a review. *Marine and Freshwater*
686 *Research* doi.org/10.1071/MF15434.
687 Hetzinger, S., Halfar, J., Kronz, A., Steneck, R.S., Adey, W., Lebednik, P. A. & Schone,
688 B. R. 2009. High-Resolution Mg/Ca Ratios in a coralline Red Alga As a Proxy
689 for Bering Sea Temperature Variations from 1902-1967. *Palaios* 24:406-412.

690 Kamenos, N., Cusack, M., & Moore, P. G. 2008. Coralline Algae Are Global
691 Paleothermometers with Bi-Weekly Resolution. *Geochimica et Cosmochimica*
692 *Acta* 72:771–779.
693 Kamenos, N. A., & Law, A. 2010. Temperature controls on coralline algal skeletal
694 growth. *J. Phycol.* 46:331-335.
695 Krayesky-Self, S., Richards, J., Rahmatian M., & Fredericq, S. 2016. Aragonite infill in
696 overgrown conceptacles of coralline Lithothamnion spp (Hapalidaceae,
697 Hapalidiales, Rhodophyta): new insights in biomineralization and
698 phylominerology. *J. Phycol.* 52:161-173.
699 Martin, C. S., Giannoulaki, M., De Leo, F., Scardi, M., Salomidi, M., Knittweis, L., Pace,
700 M. L. et al. 2014. Coralligenous and maërl habitats: predictive modelling to
701 identify their spatial distributions across the Mediterranean Sea. *Sci. Rep.* 4.
702 McCoy, S. J., & Kamenos, N. A. 2015. Coralline algae (Rhodophyta) in a changing
703 world: integrating ecological, physiological, and geochemical responses to global
704 change. *J. Phycol.* 51:6-24.
705 Nash, M.C. & Adey, W., 2017. Multiple phases of mg□calcite in crustose coralline algae
706 suggest caution for temperature proxy and ocean acidification assessment: lessons
707 from the ultrastructure and biomineralisation in Phymatolithon (Rhodophyta,
708 Corallinales). *J. Phycol*. In press. 10.1111/jpy.12559
709 Nash, M. C., Troitzsch, U., Opdyke, B., Trafford, J., Russell, B., & Kline, D. 2011. First
710 discovery of dolomite and magnesite in living coralline algae and its
711 geobiological implications. *Biogeosciences*. 8, 3331-3340.

712 Nash, M. C., Opdyke, B. N., Wu, Z., Xu, H. & Trafford J. M. 2013. Simple X-ray
713 diffraction techniques to identify Mg calcite, dolomite, and magnesite in tropical
714 coralline algae and assess peak asymmetry. *J. Sed. Res.* 83:1085-1099.
715 Nash, M. C., Uthicke, S., Negri, A.P., & Cantin, N. E. 2015. Ocean acidification does not
716 affect magnesium composition or dolomite formation in living crustose coralline
717 algae, *Porolithon onkodes* in an experimental system. *Biogeosciences* 12:5247-
718 5260.
719 Nash M.C., Martin S., Gattuso J-P. 2016. Mineralogical response of the Mediterranean
720 crustose coralline alga *Lithophyllum cabiochae* to near-future ocean acidification
721 and warming. *Biogeosciences Discussions* doi:10.5194/bg-2016-160.
722 Ragazzola, F., Foster, L. C., Jones, C. J., Scott, T. B., Fietzke, J., Kilburn, M. R., &
723 Schmidt, D. N. 2016. Impact of high CO_2 on the geochemistry of the coralline
724 algae *Lithothamnion glaciale*. *Scientific reports*, *6*, 20572.
725 Ries, J. 2010. Review: Geological and Experimental Evidence for Secular Variation in
726 Seawater Mg/Ca (Calcite-Aragonite Seas) and Its Effects on Marine Biological
727 Calcification. *Biogeosciences*, 7:2795–2849.
728 Sletten, H. R., Andrus, C. F. T., Guzmán, H. M.,, & Halfar, J. 2017. Re-evaluation of
729 using rhodolith growth patterns for paleoenvironmental reconstruction: An
730 example from the Gulf of Panama. *Palaeogeography, Palaeoclimatology,*
731 *Palaeoecology* 465:264-277.
732 Sinutok, S., Hill, R., Doblin, M. A., Kühl, M., & Ralph, P. J. 2012. Microenvironmental
733 changes support evidence of photosynthesis and calcification inhibition in
734 *Halimeda* under ocean acidification and warming. *Coral Reefs* 31:1201-1213.

735 Sherman, C.E., Fletcher, C., Rubin, K., Simmons, K. & Adey, W. 2014. Sea-level and
736 reef accretion history of Marine Oxygen Isotope Stage 7 and late stage 5 based on
737 age and facies of submerged late Pleistocene reefs, Oahu, Hawaii. *Quaternary Res*.
738 81:138-150.
739 Vásquez-Elizondo, R.M. and Enríquez, S., 2016. Coralline algal physiology is more
740 adversely affected by elevated temperature than reduced pH. *Scientific reports*, *6*,
741 p.19030.
742 Wanamaker, A., Kreutz, K., Schone, B., Pettigrew, N., Borns, H., Introne, D., Belknap,
743 D., Maasch, K. & Feindel, S. 2008. Coupled North Atlantic slope water forcing
744 on Gulf of Maine temperatures over the past millennium. *Climate Dynamics*
745 31:183-194.
746 Williamson, C. J., Najorka, J., Perkins, R., M. L. Yallop, M. L. & Brodie, J. 2014.
747 Skeletal mineralogy of geniculate corallines: providing context for climate change
748 and ocean acidification research. *Marine ecology progress series* 513:71-84.
749

750 **Tables**

	K.epilaeve		*L. laeve*					
	IF	CW	CW Under	CW Upper	CW comb.	Under Hyp.	Upper transit.	Upper Hyp.
mol% $MgCO_3$	9.1%	10.1%	11.2%	12.9%	12.2%	12.3%	15.6%	16.7%
St. Dev.	1.0%	1.2%	1.2%	2.5%	2.2%	0.7%	1.7%	1.7%
Mg/Ca	0.100	0.113	0.126	0.149	0.138	0.140	0.185	0.200

751 **Table 1: SEM-EDS results. Conversion of mol% to Mg/Ca is included.**

	Average mol% and n	*K. epilaeve* IF	*K. epilaeve* CW	*L. laeve* under CW	*L. laeve* upper CW	*L. leave CW both*	*L. laeve* under Hyp.	*L. laeve* upper Hyp.
K. epilaeve	9.1 %							

IF	n=9							
K. epilaeve CW	10.1% n=8	**0.069**						
L. laeve under CW	11.2% n=8		0.129					
L. laeve upper CW	12.9% n=9		**0.012**	0.112				
L. leave CW both	12.2% n=17		**0.024**					
L. laeve under Hyp.	12.3% n=8			**0.052**	0.470	0.914		
L. laeve upper Hyp.	16.7% n=8					**<0.001**	**<0.001**	
L. laeve upper trans.	15.6% n=8					**<0.001**	**<0.001**	0.259

Table 2: T-test *p* values for 15 kV spot EDS.

Figures

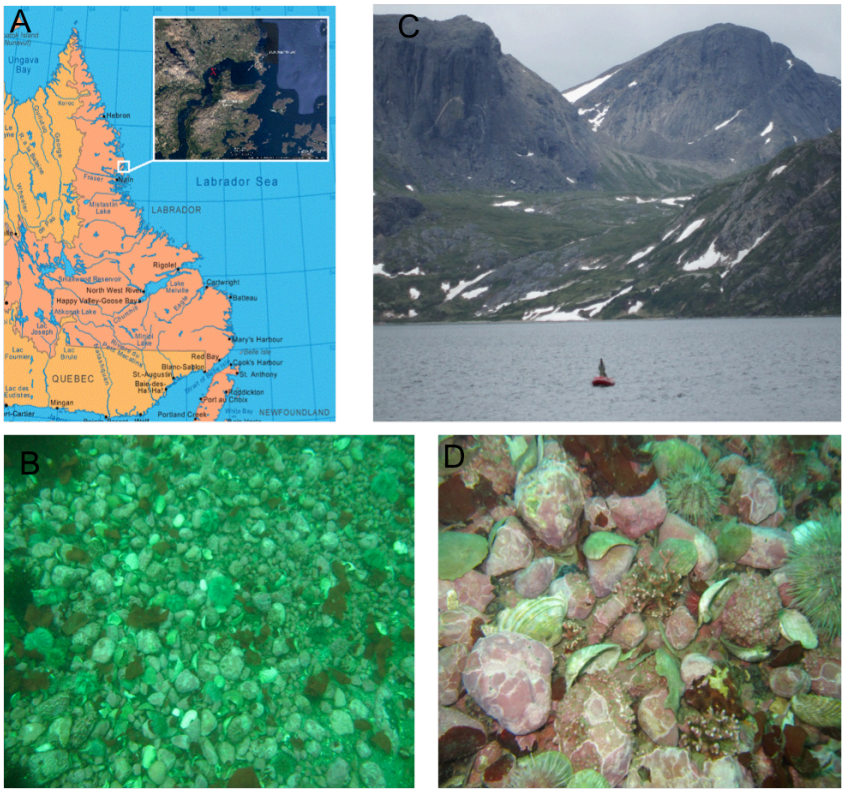

Figure 1: A. Port Manvers Bay Station, Labrador. B. Pebble/shell bottom with occasional rhodoliths at 15-17 m. Coralline covered pebbles range from about 5-10 cm diameter. C. Collecting site in western Port Manvers Bay. D. Close-up of bottom shown in figure 1C.

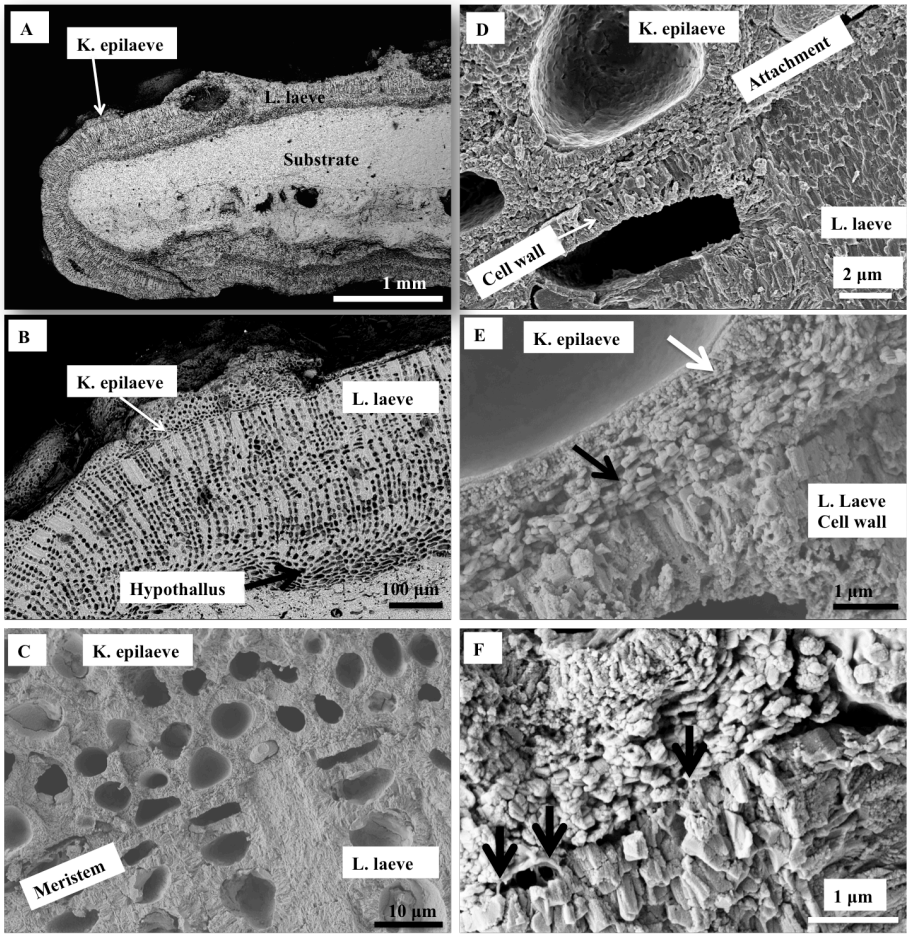

Figure 2: Overview of *K. epilaeve* on *L. laeve*. **A**. Overview (BSE). *L. laeve* has been partly overgrown by *K. epilaeve*. **B**. Closer up (BSE) *K. epilaeve* has a very thin perithallium with thicker buildup for its conceptacle. **C**. Close up (SE) and **D** showing attachment zone of *K. epilaeve* hypothallus on the meristem of the *L. laeve*. **E**. (SE) The cell wall in the *L. laeve* is roughly radial whereas the *K. epilaeve* cell wall does not appear properly mineralized with nm-scale beads of Mg-calcite along what appears to be organic fibrils (white arrow). The *K. epilaeve* Mg-calcite layer at the attachment zone has coarse angular grains roughly parallel to the *L. laeve* surface (black arrow). **F**. (SE) Organic fibrils are visible (black arrows) between the base of the *K. epilaeve* and the surface of the *L. laeve* suggesting this is the attachment mechanism.

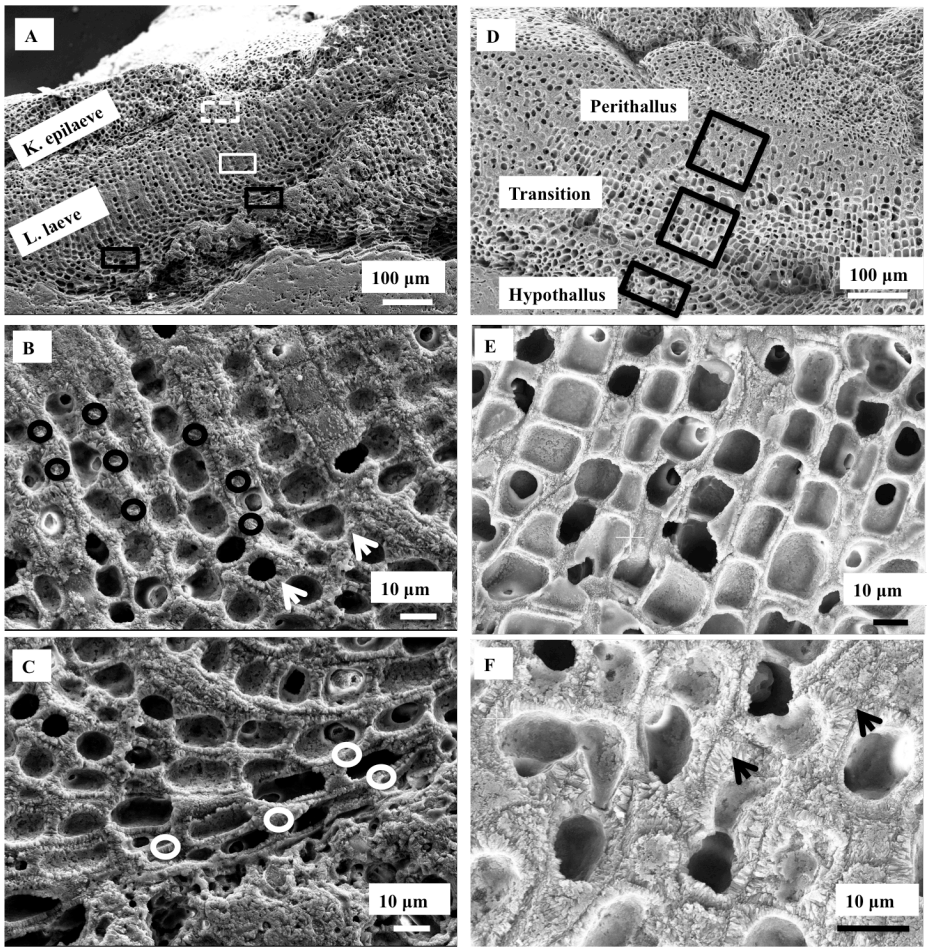

Figure 3: Overview of *L. laeve* and *K. epilaeve* and EDS sites in *L. laeve*. **A-C**. Sites on the underside of the pebble. **D-F**. Sites on the upper side of the pebble. **A**. White dashed box- cell wall and interfilament in *K. epilaeve*. White box– perithallial cell wall *L. laeve*. Black box- hypothallus *L. laeve*. **B.** EDS sites for cell wall measurements of *L. laeve*. Circle size indicates approximate area of measurement (3 microns). Cell wall radial Mg-calcite (arrowheads). **C**. EDS sites for hypothallus (right box in A). **D**. EDS sites on sample upper side for *L. laeve*. **E.** *L. leave.* **F**. *L. leave.* Cell walls in upper side are visually comparable to cell walls in underside with radial Mg-calcite (arrowheads) in cell walls and minimal interfilament.

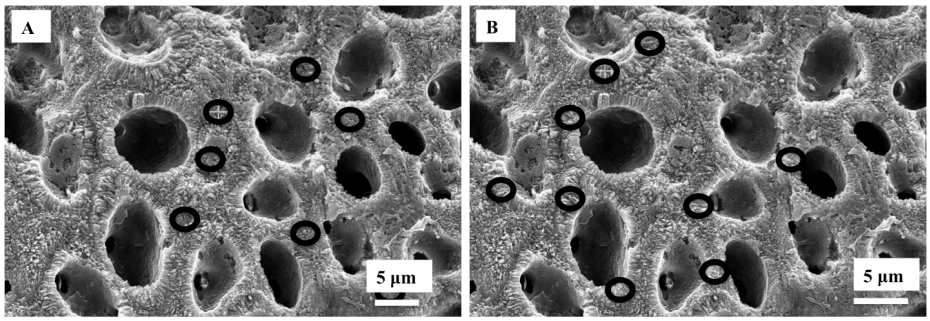

776

777 Figure 4: Detail of EDS in *K. epilaeve* (dashed white box in Fig. 2A) **A**. EDS sites for interfilament. **B**.

778 EDS sites for cell wall.

779

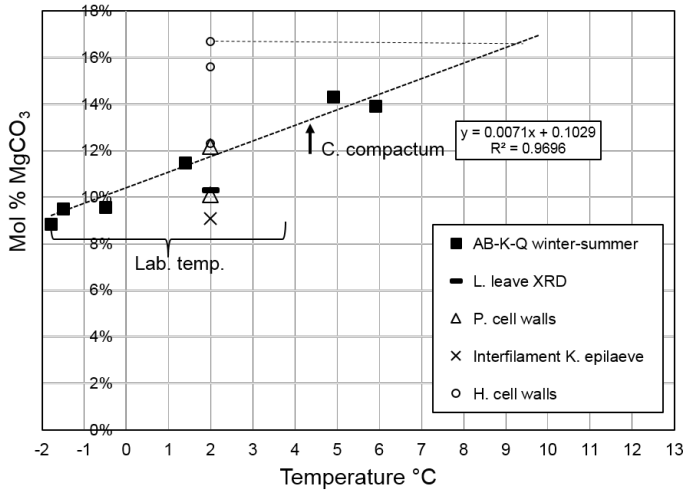

780

781 Figure 5: *L. Leave* and *K. epileave* Mg content relative to *Clathromophum compactum* from Arctic Bay,

782 Kingitok and Quirpon (Halfar et al. 2010, 2013). Lab – Labrador sea. Heavy dashed line- best fit for *C.*

783 *compactum*. Light dashed line- indicates the temperature equivalent on the *C. compactum* line for the *L.*

784 *leave* hypothallial Mg-content.

785

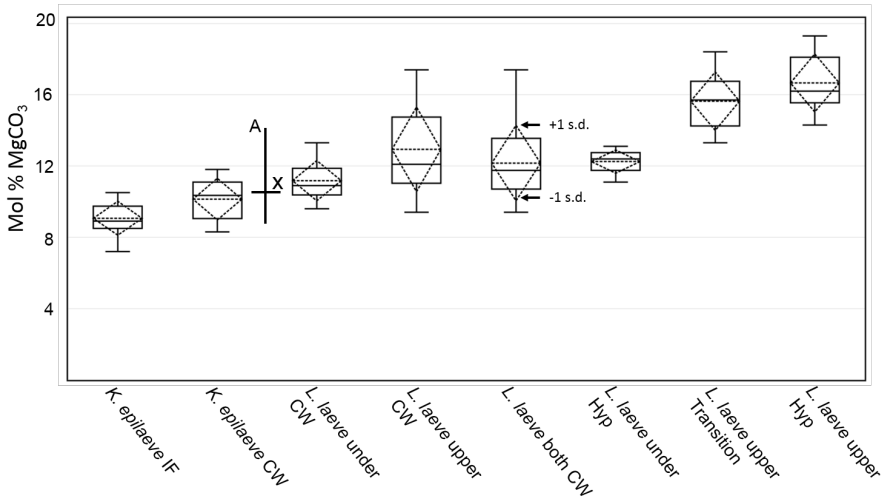

786

787 Figure 6: Box plot of EDS mol% $MgCO_3$ results. Box represents the 2nd and 3rd quartiles. The lower and
788 upper bars are the minimum and maximum values (excluding an outlier for *L. laeve* under cell wall). The
789 solid middle line within the box is the median value and the dash middle line the average. The dashed
790 diamond box represents one standard deviation. The drawn-on cross represents the XRD mol% (X) and the
791 seasonal range (A) of mol% for the Arctic Bay – Kingitok – Quirpon dataset in figure 5.

792

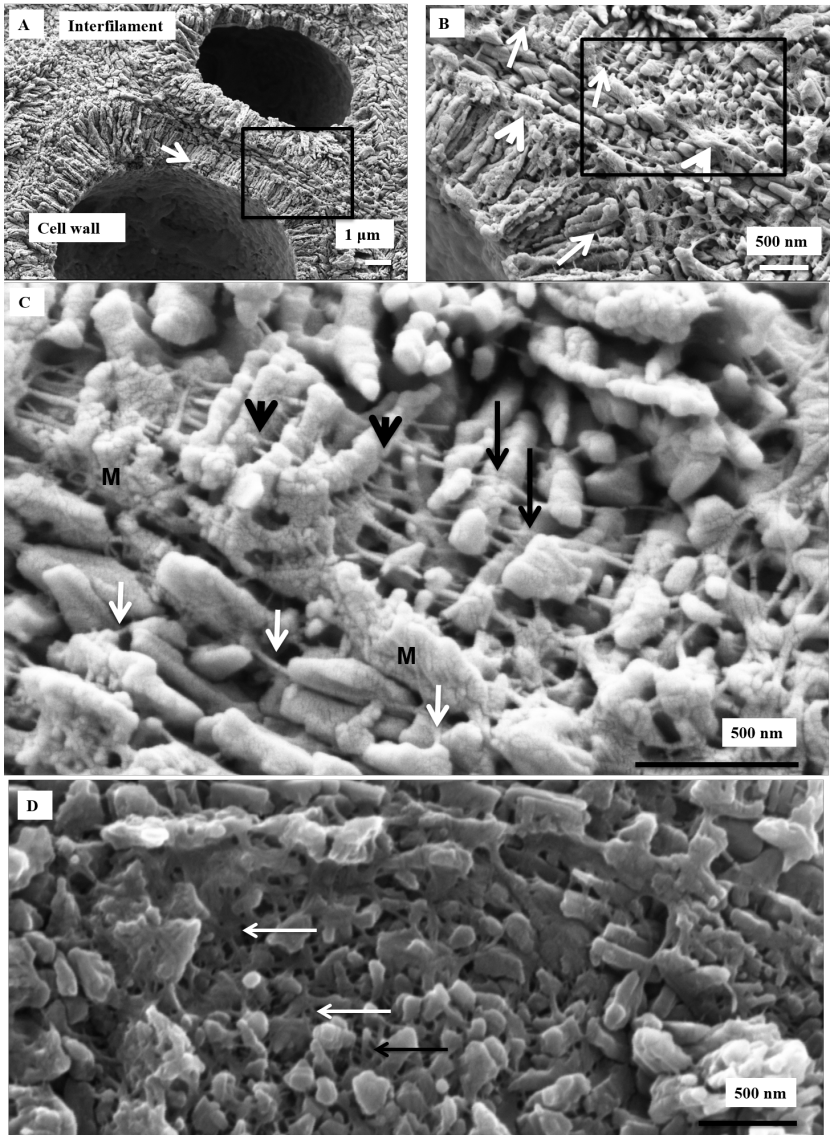

Figure 7: *K. epilaeve* cell wall structure. Crust polished and cleaned for 2 minutes. **A**. Cell walls have radial Mg-calcite whereas the interfilament grains are orientated either parallel to the filament axis or randomly within the corner junctions. Within the radial cell walls a secondary concentric banding pattern is visible (white arrow). Black box enlarged in B. **B**. Organic fibrils, ~10nm wide, run parallel to cell wall edges

798 (black arrows). Fibrils are concentrated along the outer of the cell wall (white arrows). Black box enlarged
799 in C. **C**. The cell wall fibrils appear to string through the centre of the radial grains (black arrowheads),
800 Other fibrils drape over the grains (black arrows). Fibrils are present in the interfilament (white arrows). M
801 – mineralized membrane. **D**. Plan view of cell wall grains. Organic fibrils form a dense mesh (white
802 arrows).
803

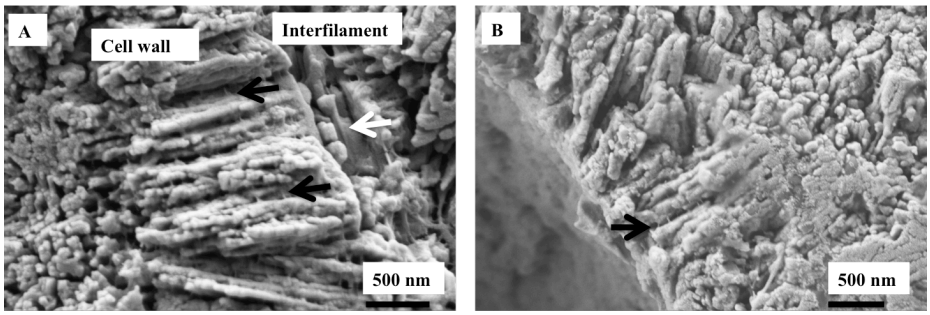

804
805 Figure 8: *L. laeve* cell wall structure. A. Cleaned for 2 minutes. Cell wall radial crystals are 1.5 micron
806 length cylindrical grains. Fibrils are present (black arrows) but not as easy to see as in the *K. epilaeve*.
807 Interfilament grains parallel to cell wall with organic fibrils (white arrows) also running parallel to cell wall.
808 B. Etched for 20 minutes. Fibrils appear similarly as in the *K. epilaeve* with the fence post-wire structure
809 (black arrows).
810

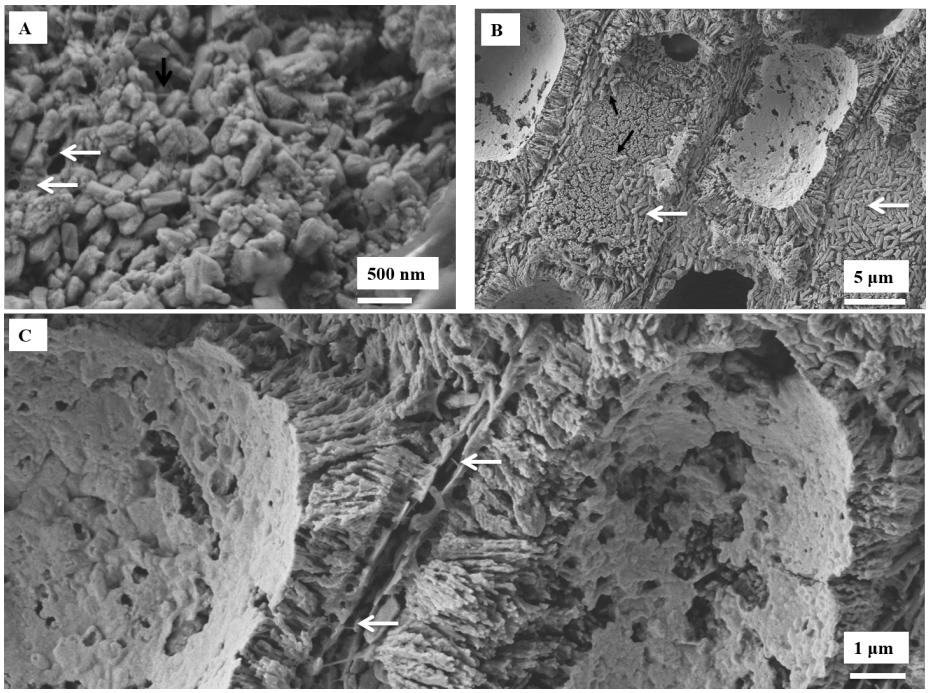

Figure 9: Interfilament structures in *K. epilaeve* (A) and *L. laeve* (B, C). **A**. *K. epilaeve* etched for 20 minutes. Fibrils (black arrow) and porous membrane (white arrows). **B**. *L. Laeve* etched for 20 minutes. Interfilament grains are flattened against the external sides of the cell wall (white arrows) attached by fibrils (black arrows). **C**. Fibrils visible stretched across the space between cell walls with 2 layers of interfilament grains (white arrows).

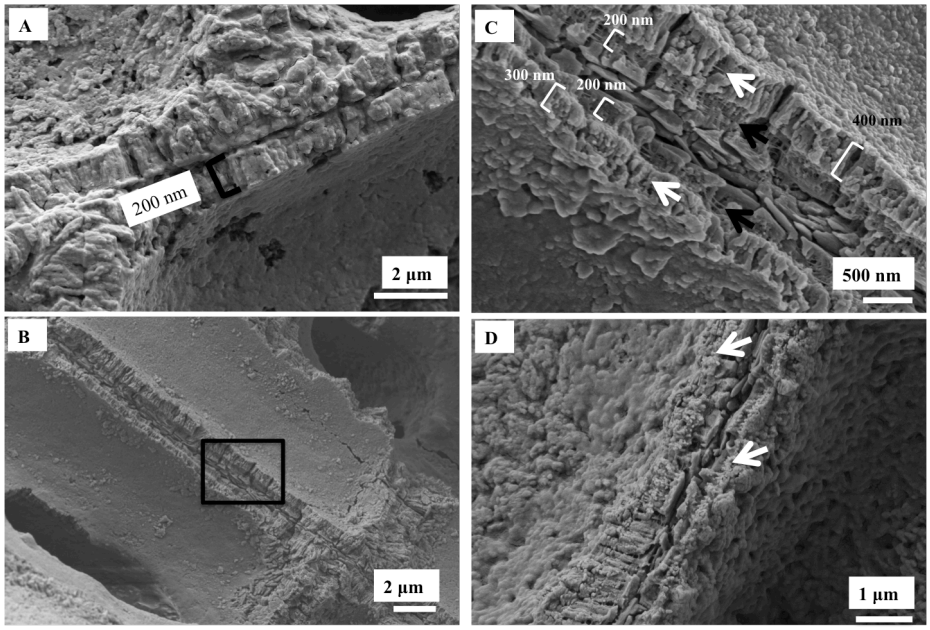

Figure 10: Hypothallus and transitional cells in *L. leave*. Cleaned 2 minutes. **A**. Hypothallus underside. Organic film covering wall structures. Walls ~200 nm wide, roughly radial structure within cell wall. **B**. Cleaned 2 minutes, hypothallus in upper crust. Roughly radial structure within cell walls. Black box enlarged in C. **C**. The wall adjacent to the interfilament is narrowest at ~200 nm, has closely spaced organic fibrils (black arrows) and is poorly calcified compared to the inner part of the wall (300-400 nm wide) where radial grains are present. There are fibrils parallel to the cell wall appearing to go through the wall grains similarly to the perithallial cell walls (white arrows). **D.** Transitional cell wall. The calcification in the lower of the left side wall is comparable to the perithallial cell wall with radial grains. The right side wall and upper part of the left side (white arrows) are poorly calcified and appear as a calcified membrane rather than a properly developed cell wall.